Journal of

Applied and Computational Mechanics

Shahid Chamran
University of Ahvaz

Research Paper

Prediction of the Supersonic Flow Base Pressure by Axisymmetric Direct Numerical Simulation

S.A. Karskanov[1], A.I. Karpov[1], A.A. Shaklein[1], A.M. Lipanov[2], I.G. Rusyak[3], S.A. Korolev[3]

[1] Udmurt Federal Research Center, Russian Academy of Science, Ural Branch, Izhevsk, 426067, Russia,
Emails: ser@udman.ru (S.A.K.), karpov@udman.ru (A.I.K.), shaklein@udman.ru (A.A.S.)

[2] Keldysh Institute of Applied Mathematics, Russian Academy of Science, Moscow, 125047, Russia, Email: aml35@yandex.ru

[3] Kalashnikov Izhevsk State Technical University, Izhevsk, 426069, Russia, Emails: primat@istu.ru (I.G.R.), stkj@mail.ru (S.A.K.)

Abstract. Axisymmetric direct numerical simulation (DNS) has been carried out to predict supersonic base flow behavior. Substantially fine grid has been used to perform calculations for the flow with Reynolds number up to 10^6. Optimal grid resolution was established through test calculations for affordable run time and solution convergence determined by the vorticity value. Numerical scheme provides fourth-order approximation for dissipative, fifth-order for convective and second-order for unsteady terms of conservation equations. Reynolds Averaged Navier-Stokes (RANS) approach has been employed to obtain input flow profiles for DNS calculations. Series of calculations have been carried out for Mach number 1.5 with Reynolds numbers 10^4, 10^5, 10^6 and for Mach number 2.46 with Reynolds number $1.65 \cdot 10^6$. It has been found that local base pressure coefficient calculated by DNS is a bit overestimated in a zone close to symmetry axis in comparison with experiment while integrated base drag coefficient shows good agreement with experimental data and noticeably better than one obtained by RANS approach.

Keywords: Compressible flow, Navier-Stokes equations, supersonic, turbulence models, partial differential equations, viscous flow.

1. Introduction

Recirculating flow formed behind the streamlined body produces a low-level pressure zone – the source of base drag. Base drag may stand for as much as an almost half of the total aerodynamic drag as it has been reported in a number of studies [1-8]. An early analysis [9] had claimed the one could amount up to 80% of total drag. There are generally accepted approaches to base drag reduction: mechanical treatments such a boat tail [1, 3, 10-12] usually applied to mass manufacturing projectiles and bullets, and base bleed arrangement [2, 13-15] for advanced missiles. In any case, a background for the proper prediction of base pressure relates to the fundamental research of turbulent wake flow downstream the blunt body. In somewhat remarkable study [3] the Navier-Stokes equations with two-layer algebraic turbulence model have been used to predict aerodynamic drag for various projectiles configurations. It has been found that such a formulation overestimates the base drag coefficient for the SOC (Secant Ogive Cylinder) and SOCBT (Secant Ogive Cylinder Boat Tail) projectile types in comparison with the measurements [16].

By now, a noticeable amount of simulations [17-22] has been carried out to predict base flow behavior. Calculations have been performed for comparison with the well-known experiment [23], which is treated generally as a test case for the evaluation of base pressure. Later, data [23] have been confirmed by another experiment [24] of the same group. Briefly, analysis of the achieved prediction results has shown the following reasoning: original RANS approach underestimates the base pressure level (correspondingly, overestimates the base drag coefficient). Further efforts employing the various sophisticated models such as RANS with compressibility correction, hybrid RANS/LES (Large Eddy Simulation) in form of DES (Detached Eddy Simulation), DDES (Delayed DES) or ZDES (Zonal DES) and PANS (Partially Averaged Navier-Stokes) significantly improve the agreement of predicted base pressure level with the measurements (for example, see recent paper [21] providing a suitable review of the up-to-date models). The considered problem could be stated as resolved since any reasonable accuracy may be obtained with the proper fitting of the correlation coefficients and functions included into the specific formulation.

In fact, there is unique available experiment for the validation of models and their polishing up based on these only data cannot vouch for the same reliability if flow parameters would be changed. In this regard, DNS approach is free from the introduction of correlation coefficients for turbulent transfer modeling, and potentially provides a way, which has a more reliable physical background. However, DNS ability to predict flow behavior with fairly high Reynolds number faces a requirement of rather fine grid resolution, which is not affordable in most practical applications, at least right now, as it is generally pointed out by the critical view [21]. The DNS calculations [5-6, 25] of supersonic wake flow have shown the reasonable estimation of base pressure coefficient for Reynolds number up to 10^5. There, both two-dimensional (axisymmetric) and three-dimensional (with spectral approach in the azimuthal direction) formulations have been carried out.

Our motivation to carry out the presented study has the following background. As it has been widely pointed out the full (three-dimensional) DNS calculations for the flow with Reynolds number of level 10^6 stand to be unachievable (right now, at least) due to unaffordable run time. Logically, predictions of such higher Reynolds number flows are performed by RANS based (including modified LES/DES approaches and numerous combinations of them) formulations, which remove grid resolution restriction. By this way, the best level of agreement between predictions and measurements could be achieved by fitting suitable empirical coefficients of subgrid turbulence model [5, 18]. These coefficients are not always physically backed up. Then, by our point of view, somewhat a remarkable study [25] provided the direct comparison between 3D and 2D-axisymmetric DNS for the base flow with Reynolds number 10^5, which showed a reasonable agreement between them. By that, we have been encouraged to make a next step, which is quite logical: perform 2D-axisymmetric DNS for the base flow with higher Reynolds number $1.65 \cdot 10^6$ as in [23]. To our experience, no such a study has been reported before. In few words, our motivation is: why not try? Which is most important, DNS approach does not need any empirical coefficients and functions as RANS-based one does.

When it comes to 2D-modeling in relation to the DNS, many critics of the approach immediately declare that this is impossible, since turbulence is purely three-dimensional. We do not argue with this, turbulence, as a physical phenomenon, is a three-dimensional process. Indeed, in the axisymmetric formulation of the problem, turbulence modeling does not occur. We define by "direct numerical simulation" modeling based on the solution of the Navier-Stokes equations without involving any empiricism, and not only calculations of turbulent flows, in which the movements of all scales present in the flow, are resolved. Speaking about direct numerical modeling based on the Navier-Stokes equations, we, in fact, turn to the study of solutions to these equations. It is obvious that in practice the axisymmetric flow is not realizable, but nothing prevents the study of the equations. We believe that such a formulation is not without meaning. It can be said that, despite the two-dimensionality of the calculation, the axisymmetric formulation does not violate the notions of the three-dimensionality of space.

A primary goal of present study is focused on the application of 2D axisymmetric DNS model to the supersonic base flow after cylinder body with the specific attention to employing such a large number of computational nodes which could be performed for a reasonable calculation time. Thus, for two-dimensional case we intentionally try to reach a maximally fine grid resolution, which, along with numerical scheme of high-order approximation, may allow to resolve the near-wall flow parameters by DNS approach.

2. Formulation and Numerical Approach

Set of governing Navier-Stokes equations formulated in non-dimensional variables for supersonic flow of a compressible gas in axisymmetric case is as follows:

$$\frac{\partial \mathbf{W}}{\partial t} + \frac{\partial \mathbf{A}}{\partial x} + \frac{\partial \mathbf{B}}{\partial r} + \frac{\mathbf{D}}{r} = 0, \tag{1}$$

where

$$\mathbf{W} = \begin{pmatrix} \rho \\ \rho u_x \\ \rho u_r \\ \rho E \end{pmatrix}, \tag{2}$$

$$\mathbf{A} = \begin{pmatrix} \rho u_x \\ \rho u_x^2 + \dfrac{p}{kM^2} - \tau_{xx} \\ \rho u_x u_r - \tau_{rx} \\ u_x \left(\rho E + \dfrac{p}{kM^2} \right) + q_x - u_x \tau_{xx} - u_r \tau_{rx} \end{pmatrix}, \tag{3}$$

$$\mathbf{B} = \begin{pmatrix} \rho u_r \\ \rho u_x u_r - \tau_{xr} \\ \rho u_r^2 + \dfrac{p}{kM^2} - \tau_{rr} \\ u_r \left(\rho E + \dfrac{p}{kM^2} \right) + q_r - u_x \tau_{xr} - u_r \tau_{rr} \end{pmatrix}, \tag{4}$$

$$\mathbf{D} = \begin{pmatrix} \rho u_r \\ \rho u_x u_r - \tau_{xr} \\ \rho u_r^2 - \tau_{rr} + \tau_{\theta\theta} \\ u_r \left(\rho E + \dfrac{p}{kM^2} \right) + q_r - u_x \tau_{xr} - u_r \tau_{rr} \end{pmatrix}, \tag{5}$$

$$E = \frac{u_x^2 + u_r^2}{2} + \frac{1}{k(k-1)M^2} \frac{p}{\rho}, \tag{6}$$

$$\tau_{xx} = \frac{2}{Re} \frac{\partial u_x}{\partial x} - \frac{2}{3Re} \nabla \cdot \mathbf{u}, \tag{7}$$

$$\tau_{rx} = \tau_{xr} = \frac{1}{\text{Re}}\left(\frac{\partial u_r}{\partial x} + \frac{\partial u_x}{\partial r}\right), \tag{8}$$

$$\tau_{rr} = \frac{2}{\text{Re}}\frac{\partial u_r}{\partial r} - \frac{2}{3\text{Re}}\nabla \cdot \mathbf{u}, \tag{9}$$

$$\tau_{\theta\theta} = \frac{2}{\text{Re}}\frac{u_r}{r} - \frac{2}{3\text{Re}}\nabla \cdot \mathbf{u}, \tag{10}$$

$$q_x = -\frac{1}{(k-1)\text{Re}\,\text{Pr}\,\text{M}^2}\frac{\partial \text{T}}{\partial x}, \tag{11}$$

$$q_r = -\frac{1}{(k-1)\text{Re}\,\text{Pr}\,\text{M}^2}\frac{\partial \text{T}}{\partial r}, \tag{12}$$

$$\nabla \cdot \mathbf{u} = \frac{\partial u_x}{\partial x} + \frac{\partial u_r}{\partial r} + \frac{u_r}{r}. \tag{13}$$

Boundary conditions are formulated according to the arrangement of computational domain shown in Fig. 1:
Inlet ($x = 0$):

$$\mathbf{W} = \mathbf{W}(r), \tag{14}$$

Outlet ($x = 8$):

$$\partial \mathbf{W}/\partial x = 0, \tag{15}$$

Free stream ($r = 4$) [26]:

$$\frac{\partial \mathbf{W}}{\partial t} + (c + u_r)\frac{\partial \mathbf{W}}{\partial r} = 0, \tag{16}$$

Symmetry axis ($r = 0$):

$$\partial \mathbf{W}/\partial r = 0, \quad u_r = 0, \tag{17}$$

Solid surface ($x = 1$ and $r = 1$):

$$u_x = 0, \quad u_r = 0, \quad \partial \rho/\partial n = 0, \quad \partial E/\partial n = 0. \tag{18}$$

It has been realized that afterbody flow in the base zone has essentially three-dimensional behavior. Our argumentation on the application of the axisymmetric formulation is that, unlike the Cartesian coordinate system, axisymmetric one allows to resolve the azimuthal shear stress $\tau_{\theta\theta}$ (Eq. (10)). Thus, three dimensional expansion of flow from the symmetry axis to outer region is actually taken into account. Similar approach [27] showing that the base flow under zero attack angle is formed mostly by longitudinal and radial velocity components.

While the most of boundary conditions presented above are rather generally accepted, special attention is to be devoted to input flow profiles. As it has been discussed [24], choice of inflow parameters significantly affects the afterbody base flow behavior. Even if the turbulent flow is approved as an ultimate decision, an assignment of boundary layer thickness and specific velocity distribution leaves a room for some uncertainty. Here, preliminary calculations for upstream flow ($x < 0$ as shown in Fig. 1) have been carried out using ANSYS Fluent software by RANS approach with SST $k - \omega$ turbulence model [28]. The ogive geometry is chosen close to M549 projectile shape [3] normalized in size to corresponding Reynolds number. Thus, distributions of flow parameters achieved form RANS simulations at the $x = 0$ cross-section are assigned as initial profiles for DNS calculations.
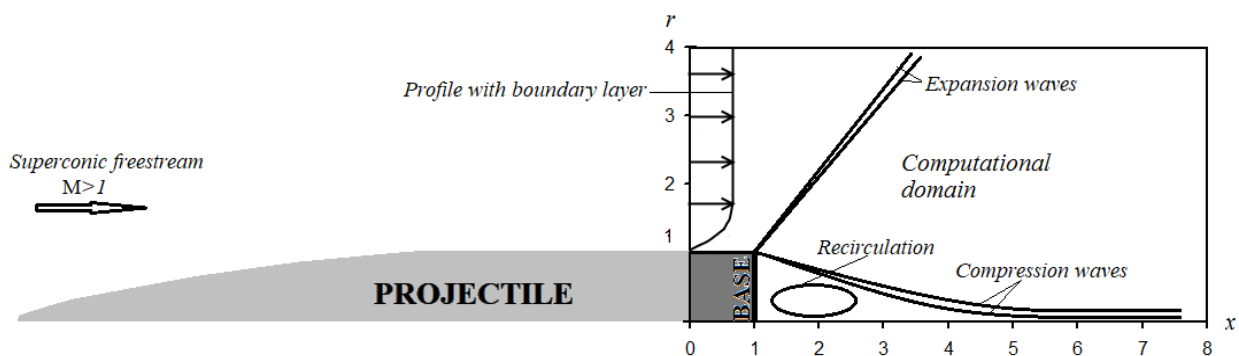

Fig. 1. Configuration of the computational domain.

In-house codes have been developed to perform DNS predictions, which have been applied timely to various transition and turbulent flows [29-30]. For the present case of base flow, the following numerical approaches are employed to Eq. (1). The coordinates system (x, r) of non-uniform grid has been conformally mapped on the coordinates (ξ, η) of uniform grid. Convective term is approximated by central differences $(\partial f / \partial \xi)_i = (f_{i+1/2} - f_{i-1/2}) / \Delta \xi$ and fifth-order WENO algorithm [31] is used as follows:

$$f_{i+1/2} = \sum_{\nu=1}^{3} \Omega^{(\nu)} f_{i+1/2}^{(\nu)}, \tag{19}$$

where $\Omega^{(1)} = 1/10$, $\Omega^{(2)} = 6/10$, $\Omega^{(3)} = 3/10$ are the weighting coefficients and f is generalized variable according to Eq. (1), which components are calculated through its neighboring nodes:

$$f_{i+1/2}^{(\nu)} = \begin{cases} f_{i+1/2}^{(1)} = \dfrac{11}{6} f_i - \dfrac{7}{6} f_{i-1} + \dfrac{2}{6} f_{i-2} \\[2mm] f_{i+1/2}^{(2)} = \dfrac{2}{6} f_{i+1} + \dfrac{5}{6} f_i - \dfrac{1}{6} f_{i-1} \\[2mm] f_{i+1/2}^{(3)} = -\dfrac{1}{6} f_{i+2} + \dfrac{5}{6} f_{i+1} + \dfrac{2}{6} f_i \end{cases}. \tag{20}$$

WENO scheme sets the weights of linear combination to be small for the domains containing discontinuity and to be close to optimal weights $\Omega^{(\nu)}$ for smooth solution:

$$f_{i+1/2}^{opt} = \sum_{\nu=1}^{3} \omega^{(\nu)} f_{i+1/2}^{(\nu)}, \tag{21}$$

$$\omega^{(\nu)} = \frac{\sigma^{(\nu)}}{\sigma^{(1)} + \sigma^{(2)} + \sigma^{(3)}}, \tag{22}$$

$$\sigma^{(\nu)} = \frac{\Omega^{(\nu)}}{\left(\varepsilon + IS^{(\nu)}\right)^a}. \tag{23}$$

Here $IS^{(\nu)}$ is indicator of smoothness [32], $a = 2$ and ε is regularizing factor (set to 10^{-6}):

$$IS^{(1)} = \frac{13}{12}\left(f_{i-2} - 2f_{i-1} + f_i\right)^2 + \frac{1}{4}\left(f_{i-2} - 4f_{i-1} + 3f_i\right)^2, \tag{24}$$

$$IS^{(2)} = \frac{13}{12}\left(f_{i-1} - 2f_i + f_{i+1}\right)^2 + \frac{1}{4}\left(f_{i-1} - f_{i+1}\right)^2, \tag{25}$$

$$IS^{(3)} = \frac{13}{12}\left(f_i - 2f_{i+1} + f_{i+2}\right)^2 + \frac{1}{4}\left(3f_i - 4f_{i+1} + f_{i+2}\right)^2. \tag{26}$$

Dissipative term is approximated by the fourth-order central differences:

$$\frac{\partial^2 f_i}{\partial \xi^2} = \frac{\sum\limits_{m=1}^{2} \beta_m \left(f_{i+m} - 2f_i + f_{i-m}\right)}{\Delta \xi^2} + O\left(\Delta \xi^4 \frac{\partial^6 f_i}{\partial \xi^6}\right), \tag{27}$$

where $\beta_1 = 4/3$, $\beta_2 = 1/12$.

Non-stationary term is integrated by second-order TVD (Total Variation Diminishing) Runge-Kutta scheme [33]:

$$W^{(1)} = W^n + \Delta t L(W^n), \tag{28}$$

$$W^{(n+1)} = \frac{1}{2} W^n + \frac{1}{2} W^{(1)} + \frac{1}{2} \Delta t L(W^{(1)}), \tag{29}$$

where L is finite-difference approximation. For an explicit scheme, the assignment of step for time integration is determined through the preliminary calculations runs providing the computational stability. Such a requirement stands to be stricter than of Courant-Friedrichs-Lewy, which set a necessary, but not a sufficient condition.

The approximation order is set to fourth, which was approved by the parametric study [34]. The same order of spatial approximation has been resulted from [24]. The series of testing calculations have been carried out for the determination of optimal grid resolution relating to the prediction reliability of the core flow parameters. Mach and Reynolds numbers are set to 2.46 and $1.65 \cdot 10^6$ respectively, number of nodes varies from 1.56 to 56 million and evaluation parameter is vorticity of averaged velocity field, which is expressed as:

$$\omega = \frac{\partial u_r}{\partial x} - \frac{\partial u_x}{\partial r}. \tag{30}$$

As for the description of base flow behavior itself, a base pressure coefficient is commonly used, which is defined as:

$$C_p = \frac{2\left(p_b / p_0 - 1\right)}{k M^2}. \tag{31}$$

Table 1. Grid arrangement.

Area	Number of nodes	Grid type
$0 < x < 1$	2000	Uniform
$1 < x < 8$	6000	Non-uniform
$0 < r < 1$	2000	Uniform
$1 < r < 4$	1500	Non-uniform

From the practical viewpoint of engineering analysis, the integrated aerodynamic base drag coefficient is involved, which is defined as:

$$C_b = -\frac{1}{S_b} \int_S C_P(r) dS, \tag{32}$$

where C_P is determined by Eq. (31).

Figure 2a presents the correlation between minimal and maximal vorticity values and number of grid nodes. It has been found that there is no actual difference of vorticity between 56 and 24 million nodes, so the latter number may be concluded as an appropriate grid resolution for the present flow conditions. Therefore, the integral parameter C_b (Fig. 2b) defined by Eq. (32), being an overall characteristic of the base drag, also shows similar convergence upon the grid resolution.

Following above reasoning, the parameters of grid arrangement corresponding to Fig. 1 are presented in Table 1. For non-uniform type a grid step increases gradually as coordinate (x or r) increases. Thus, total number of nodes involved into the calculations is $N = (8000 \times 3500) - (2000 \times 2000) = 24 \cdot 10^6$.

Furthermore, the capability to predict near-wall turbulent flow has to be evaluated. Since DNS approach is employed here, generally used near-wall function treatment could not be engaged. Thus, Fig. 3 presents the values of the non-dimensional wall distance y^+ at the first near-wall node both along the cylinder surface ahead of baseline ($r^+, 0 < x < 1$ in Fig. 1) and along the baseline ($x^+, 0 < r < 1$ in Fig. 1). It has been established [35] that viscous sublayer is located nearby the surface at distance of $y^+ < 5$. For industrial turbulent flows [36], which commonly has a non-trivial configuration, the value of $y^+ \sim 2$ is considered to ensure the proper resolution of viscous sublayer. As data of Fig. 3 have shown, these conditions are satisfied here.
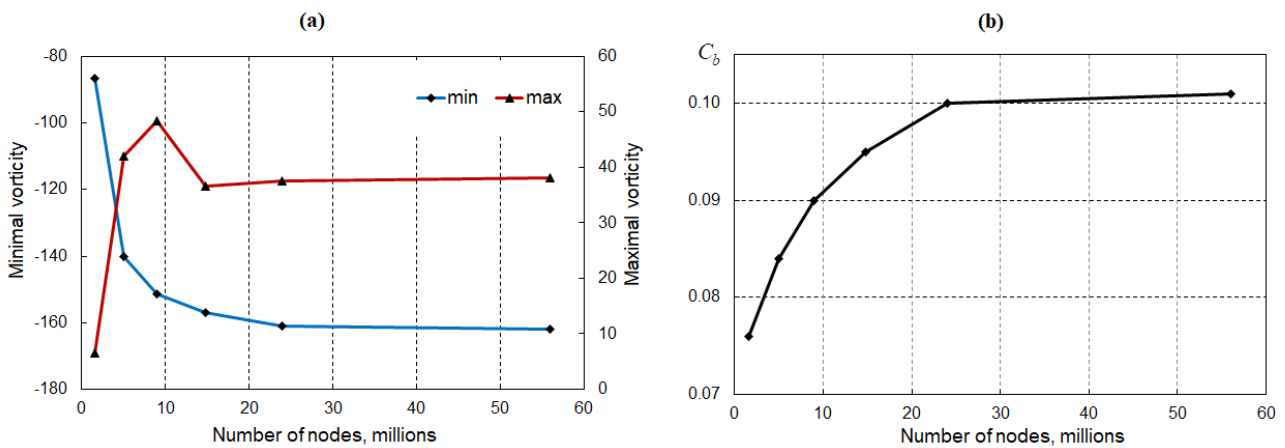

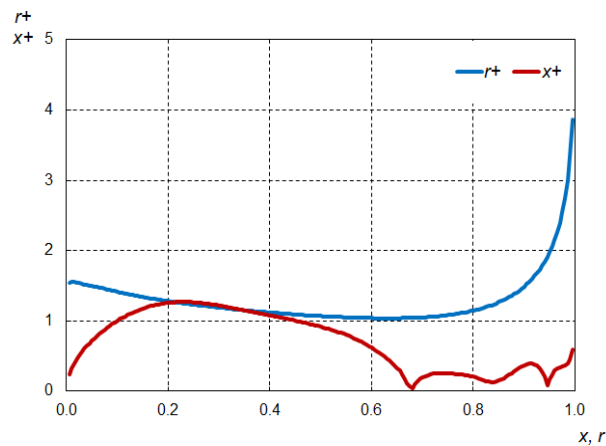**Fig. 2.** Validation of convergence: (a) vorticity, (b) integral base drag coefficient.

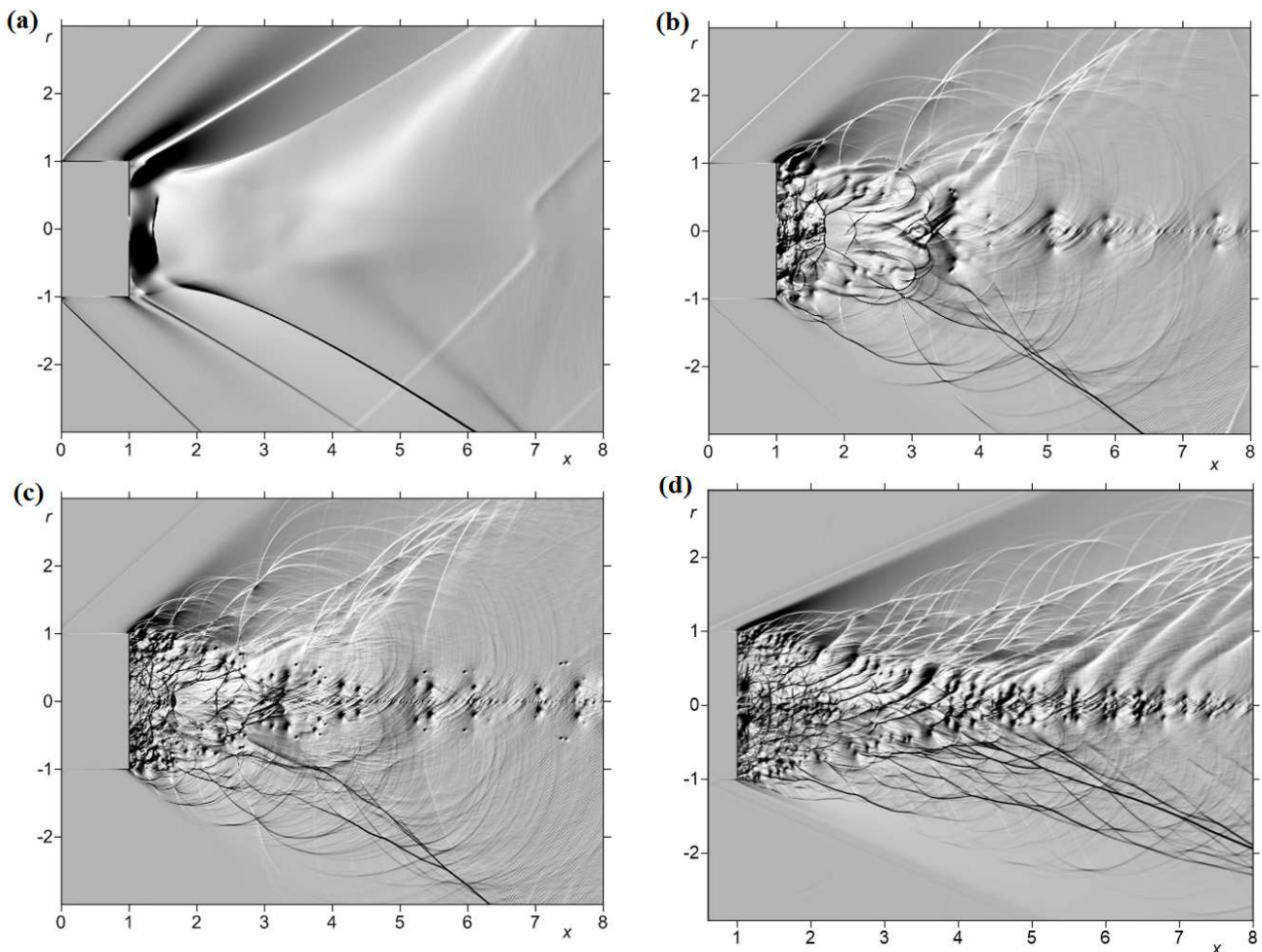**Fig. 3.** Distribution of wall distance at the first near-wall node.

Fig. 4. Schlieren images of instantaneous pressure field at: (a) Re = 10^4, M = 1.5 (b) Re = 10^5, M = 1.5 (c) Re = 10^6, M = 1.5 (d) Re = 1.65×10^6, M = 2.46.
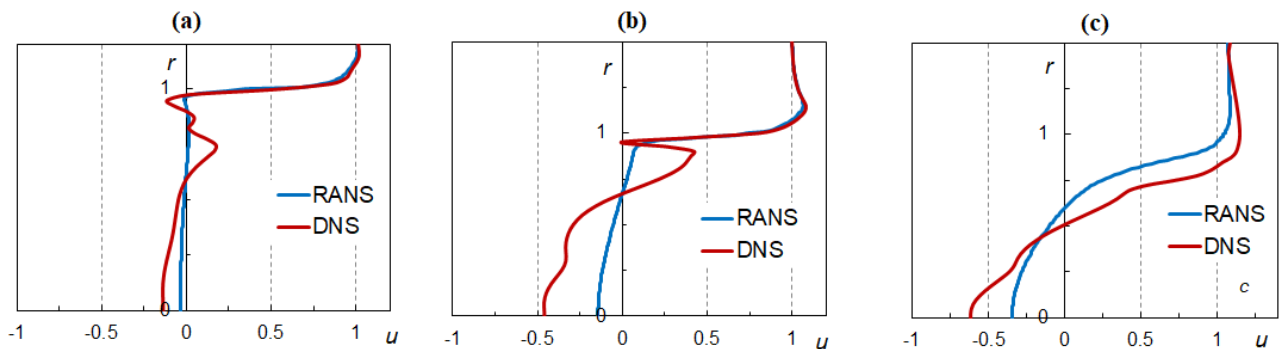

Fig. 5. Distribution of axial velocity profiles at Re = 10^4, M = 1.5: (a) $x = 1.05$, (b) $x = 1.2$, (c) $x = 2.0$.

3. Results and Discussion

As reported previously [3, 9], the maximal base drag coefficient is observed around Mach number of 1.2…1.5. Figure 4 presents the pressure distribution for Mach number $M = 1.5$ and various Reynolds numbers. The viscous factor of dissipative terms has higher effect under the lower Reynolds number. Thus, under Reynolds number of 10^4 the flow in recirculation zone has almost laminar behavior forming no-vortex jet (Fig. 4a). As rather expected the flow shows a vivid pulsating behavior with the increasing of Reynolds number, where viscous effect drops, which results in flow field is affected by number of interacting shock waves with intensive turbulization (Figs. 4b and 4c). It has been found that for a given grid resolution indicated in Table 1 and numerical scheme of approximation orders specified above, present DNS calculations show persistent character of computational procedure for Reynolds number up to 10^6. As for the higher Reynolds number (trial case for Re = 10^7 has been tested), a noticeable numerical instability emerges and more number of nodes and/or higher order of approximation are required.

Distributions of axial velocity profiles for various Reynolds and Mach numbers are shown in Figs. 5-8, where results of DNS calculations are compared with RANS ones. Here, RANS calculations have been carried out using ANSYS Fluent with SST $k - \omega$ turbulence model [28]. While the RANS approach provides almost the same flow structure for all the Reynolds numbers under consideration, the DNS exhibits a different behavior. The smallest difference between them occurs in the zone very close to the base surface ($x = 1.05$). For Re = 10^4 (Fig. 5a) the velocity profiles are qualitatively similar but the sizes of recirculating zones are greater in magnitude in the case of DNS.
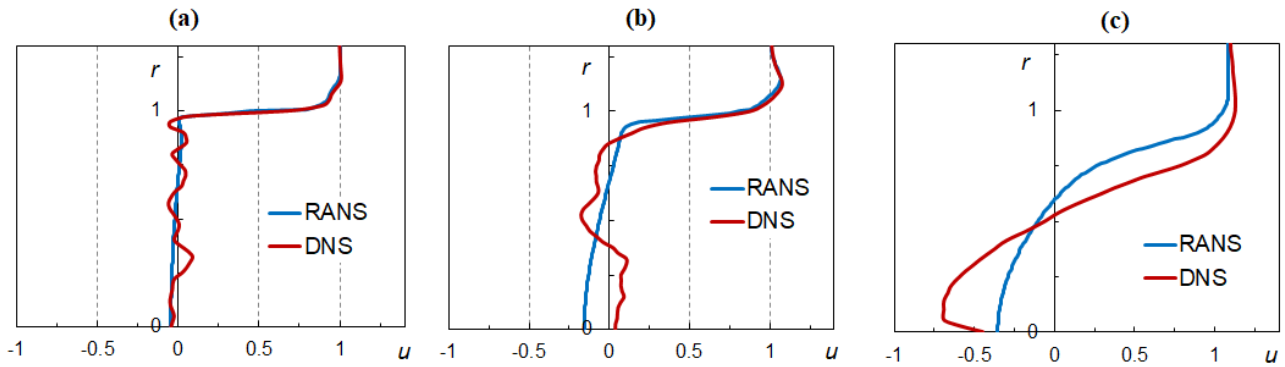
Fig. 6. Distribution of axial velocity profiles at Re = 10^5, M = 1.5: (a) x = 1.05, (b) x = 1.2, (c) x = 2.0.
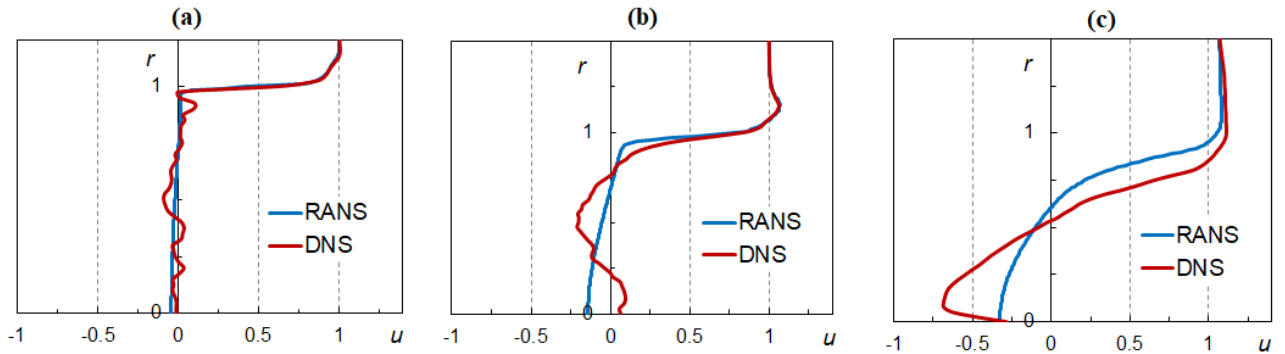

Fig. 7. Distribution of axial velocity profiles at Re = 10^6, M = 1.5: (a) x = 1.05, (b) x = 1.2, (c) x = 2.0.
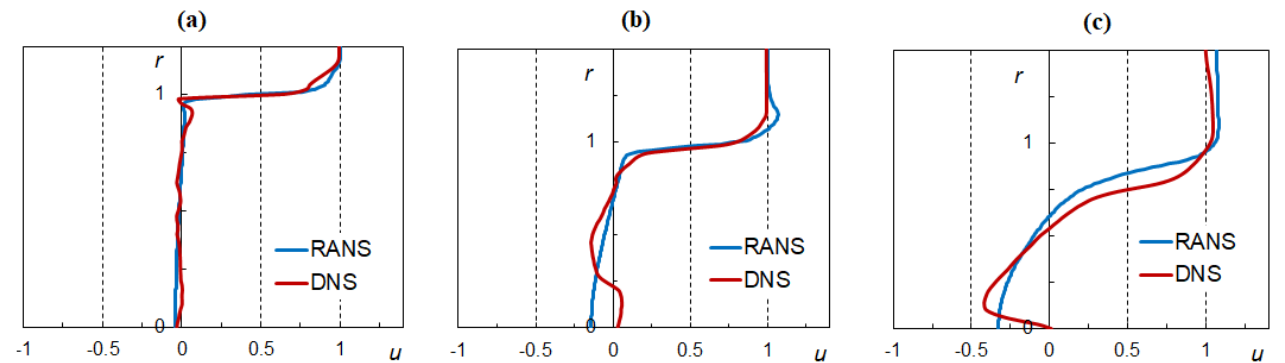

Fig. 8. Distribution of axial velocity profiles at Re = 1.65×10^6, M = 2.46: (a) x = 1.05, (b) x = 1.2, (c) x = 2.0.

When the Reynolds number becomes greater than 10^4 and the viscosity forces become smaller, the flow behind the streamlined body becomes strongly perturbed. DNS profiles near the wall become nonmonotonic. The data in Fig. 4 testify to the same. RANS profiles look almost like a straight line. Generally, such a peculiarity is rather explainable because of the small-scale vortices are damped by turbulent viscosity close to base wall introduced in RANS models (in lesser extent the same occurs under various modifications of combined RANS/LES approach as it has been shown previously) [18, 21].

At the cross-section $x = 1.2$, a secondary vortex around symmetry axis is formed for $Re = 10^5$ (Fig. 6b) and $Re = 10^6$ (Fig. 7b). Furthermore, as the observation point moves away from the base (Fig. 5c, Fig. 6c, Fig. 7c, Fig. 8c), the DNS results in the vicinity of $r = 0$ are more distant from the RANS velocity profiles. The size of the recirculation zone becomes larger for the DNS approach. The axisymmetric formulation begins to have a negative effect. It becomes obvious that it will not be possible to establish the point of attachment of the recirculation zone with an acceptable accuracy using an axisymmetric DNS. However, the parameters near and at the boundary of the streamlined body, which are most important for practice and engineering, are simulated quite reliably.

Figure 9 presents the distributions of base pressure coefficient along the radial coordinate for various Reynolds numbers. It has to be noted that there is a common unwanted feature of DNS results (reported also in previous studies [5, 25], which is an over-estimation of base pressure near the symmetry axis. There is a consequence of the fact that azimuthal components of the stress tensor could not be resolved properly by axisymmetric model in this area of weak flow expansion in radial direction. This effect appears most evidently for low Reynolds number 10^4 (Fig. 9a). As turbulent mixing intensifies with the increasing of Reynolds number (Fig. 9b), shortcoming of base pressure distribution becomes not so crucial. Meaning of the fact that essentially turbulent flow regime is the point of interest for present study, achieved evaluation of base pressure may be concluded relevant enough.
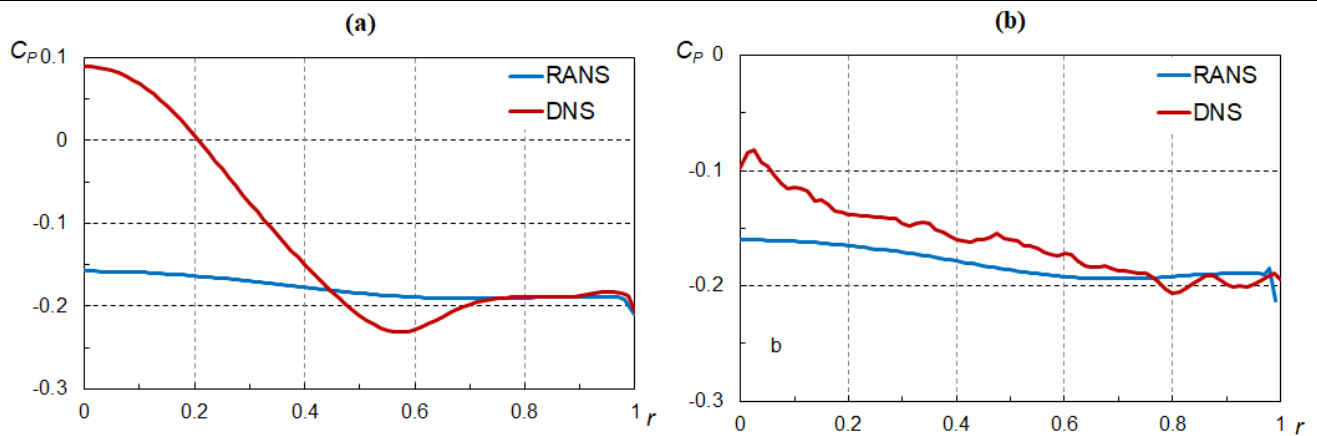
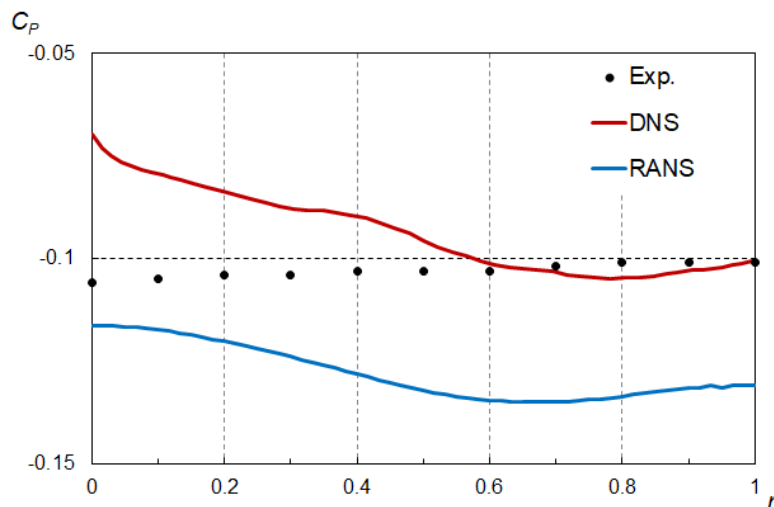**Fig. 9.** Distribution of base pressure coefficient, M = 1.5: (a) Re =10^4, (b) Re = 10^5.

Fig. 10. Distribution of base pressure coefficient at Re = $1.65×10^6$ and M = 2.46; exp. – Herrin and Dutton [23], curves DNS and RANS – present calculations.

Distribution of base pressure coefficient for $\text{Re} = 1.65 \cdot 10^6$ and $\text{M} = 2.46$ available from the experiment [23] is presented in Fig. 10.

These data show the increased value of base pressure on the centerline. The origin of such a disagreement refers to the used two-dimensional axisymmetric approach which is hardly able to predict flow parameters on the symmetry axis with higher accuracy since azimuthal dissipative momentum transfer has to be taken into account to decrease the axial momentum as is carried out in 3D formulation. However, in comparison with the very similar two-dimensional axisymmetric DNS calculations [5] performed on the rather coarse grid, present peak of base pressure stands to be much lower. Values of the base drag coefficient presented in Table 2 provide the clear evidence of presented approach reliability to predict base flow behavior.

In addition, it should be borne in mind that the closer the point is to the axis, the smaller its contribution to the general integral. Therefore, the divergences of the C_P values caused by the axisymmetric model near the axis have little effect on the value of the general integral (that is, the total base drag).

The dependence of base drag coefficient upon the Reynolds number presented in Table 2 assures that its evaluation obtained through RANS approach exceeds slightly the values achieved by DNS. Since the data [3, 21] showed underestimation of base pressure (correspondingly, overestimation of integrated base drag coefficient) for RANS calculations, some tendency to better DNS predictions may be concluded. Actually, the data of Fig. 10 would ensure that proper selection of turbulence model coefficients and functions provides any reasonable agreement with the experiment (in addition to Fig. 10 data see [18] for widest modifications of RANS/LES/DES approaches).

Thus, the performed calculations and analysis testify to the viability of DNS as a method for studying even real high-speed flows. Of course, the axisymmetric model imposes significant limitations on simulation. It is not possible to obtain exact values of parameters on the axis, such as the point of attachment, the dimensions of the recirculation zone. On the other hand, it is obvious that the results, which are so close to the experimental data, were obtained under the action of physical rather than scheme viscosity, even for Re of the order of 10^6.

Table 2. Integrated base drag coefficient.

Mach number	1.5	1.5	1.5	2.46
Reynolds number	10^4	10^5	10^6	$1.65·10^6$
Present RANS	0.1950	0.2004	0.1922	0.117
Present DNS	0.1876	0.1904	0.1787	0.100
Experiment	-	-	0.18±0.02 (Chapman [9])	0.103 (Herrin and Dutton [23])

4. Conclusion

Generally, application of original RANS approach for the analysis of base flow provides substantial underestimation of base pressure in comparison with experimental data. Further efforts based on employing the various sophisticated models for averaged equations (e.g. PANS [21]) significantly improve the agreement of predicted results with the measurements, and in fact, any reasonable accuracy may be obtained with the proper fitting of the correlation coefficients and functions included into the specific formulation. However, in some sense, such a methodology limits the capability of computer modeling as a self-contained research tool since no one can vouch for reliability of developed technique in the case of flow conditions other than ones at which the model was calibrated. In this regard, DNS approach does not need the introduction of correlation coefficients and functions for turbulent transfer modeling, but faces the great challenge of computational resource demands. To obtain the affordable calculation run time the axisymmetric DNS formulation with high-order approximations have been employed in present study. Through the test parametric predictions, the optimal grid resolution has been established, which provides both reasonable computation time and convergence of numerical solution. The application of proposed approach to the investigation of base flow behavior showed reasonable agreement of predicted results with the experimental data.

Author Contributions

S. Karskanov numerically simulated the considered mathematical model. A. Karpov formulated the concept and wrote original text. A. Shaklein evaluated the methodology. A. Lipanov developed the mathematical DNS model. I. Rusyak and S. Korolev validated the results and performed RANS calculations. All authors discussed and analyzed the results, approved the final version of the manuscript

Acknowledgments

Conflict of Interest

The authors declared no potential conflicts of interest concerning the research, authorship, and publication of this article.

Funding

Data Availability Statements

Not Applicable.

Nomenclature

a, ε	Regularizing factors	r	Dimensionless radial coordinate
c	Dimensionless sonic velocity	Re	Reynolds number
C_B	Base drag coefficient	t	Dimensionless time
C_P	Base pressure coefficient	T	Dimensionless temperature
E	Relative energy	u	Dimensionless velocity
f	Generalized variable, flux function	**W, A, B, D**	Algebraic vectors
$IS^{(v)}$	Indicator of smoothness	x	Dimensionless axial coordinate
k	Adiabatic index	y^+	Non-dimensional wall distance
M	Mach number	θ	Azimuthal direction
n	Normal direction	ρ	Dimensionless density
N	Number of nodes	τ	Viscous stress tensor
p	Dimensionless pressure	ξ, η	Uniform grid directions
Pr	Prandtl number	ω	Vorticity
q	Heat flux	$\Omega(\nu)$	Weighting coefficient

References

[1] Compton III, W.B., Effect on Base Drag of Recessing the Bases of Conical Afterbodies at Subsonic and Transonic Speeds, *NASA Technical Note D-4821*, 1968.

[2] Sahu, J, Nietubicz, C.J, Steger, J.L., Navier-Stokes Computations of Projectile Base Flow with and without Mass Injection, *AIAA Journal*, 23(9), 1985, 1348-1355.

[3] Sahu, J., Drag Predictions for Projectiles at Transonic and Supersonic Speeds, *Memorandum Report BRL-MR-3523*, 1986.

[4] Rollstin, L., Measurement of In-Flight Base Pressure on an Artillery-Fired Projectile, *AIAA Paper 87-2427*, 1987.

[5] Fasel, H.F., Sandberg, R.D., Simulation of Supersonic Base Flows: Numerical Investigations Using DNS, LES and URANS, *Report ARO Grant No. DAAD190210361*, 2006.

[6] Sandberg, R.D., Fasel, H.F., Direct Numerical Simulations of Transitional Supersonic Base Flows, *AIAA Journal*, 44(4), 2006, 848-858.

[7] Reddy, D.S.K., Sah, P., Sharma, A., Prediction of Drag Coefficient of a Base Bleed Artillery Projectile at Supersonic Mach number, *Journal of Physics: Conference Series*, 2054, 2021, 012013.

[8] Aziz, M., Ibrahim, A., Riad, A., Ahmed, M.Y.M., Live Firing and 3D Numerical Investigation of Base Bleed Exit Configuration Impact on Projectile Drag, *Advances in Military Technology*, 17(1), 2022, 137–152.

[9] Chapman, D.R., An Analysis of Base Pressure at Supersonic Velocities and Comparison with Experiment, *NACA Technical Note 2137*, 1950.

[10] McCoy, R.L., MC DRAG – A Computer Program for Estimating the Drag Coefficients of Projectiles, *Technical Report ARBRL-TR-02293*, 1981.

[11] Karpov, B.G., The Effect of Various Boattail Shapes on Base Pressure and Other Aerodynamic Characteristics of a 7-Caliber Long Body of Revolution at M=1.70, *Report No. 1295 US Army Ballistic Research Laboratory*, 1965.

[12] Mair, W.A., Reduction of Base Drag by Boat-Tailed Afterbodies in Low-Speed Flow, *Aeronautical Quarterly*, 20(4), 1969, 307-320.

[13] Sahu, J., Heavey, K.R., Numerical Investigation of Supersonic Base Flow with Base Bleed, *AIAA Paper 95-3459*, 1995.
[14] Mathur, T., Dutton, J.C., Velocity and Turbulence Measurements in a Supersonic Base Flow with Mass Bleed, *AIAA Journal*, 34(6), 1996, 1153-1159.
[15] Kubberud, N., Øye, I.J., Extended Range of 155mm Projectile Using an Improved Base Bleed Unit, *Simulations and Evaluation, 26th International Symposium, DEStech Publications*, 2011, 549-560.
[16] Kayser, L.D., Base Pressure Measurements on a Projectile Shape at Mach Numbers from 0.91 to 1.20, *Memorandum Report ARBLR-MR-03353*, 1984.
[17] Forsythe, J.R., Hoffmann, K.A., Cummings, R.M., Squires, K.D., Detached-Eddy Simulation with Compressibility Corrections Applied to a Supersonic Axisymmetric Base Flow, *Journal of Fluids Engineering*, 124(4), 2002, 911-923.
[18] Simon, F., Deck, S., Guillen, P., Sagaut, P., Reynolds-Averaged Navier-Stokes/Large-Eddy Simulations of Supersonic Base Flow, *AIAA Journal*, 44(11), 2006, 2578-2590.
[19] Garbaruk, A., Shur, M., Strelets, M., Travin, A., Supersonic Base Flow, *in: DESider – A European Effort on Hybrid RANS-LES Modelling*, W. Haase, M. Braza, A. Revell (Eds.), Notes on Numerical Fluid Mechanics and Multidisciplinary Design, Springer, Vol.103, 2009, 197-206.
[20] Shin, J.R., Choi, J.Y., DES Study of Base and Base-Bleed Flows with Dynamic Formulation of DES Constant, *AIAA Paper 2011-662*, 2011.
[21] Luo, D., Yan, C., Wang, X. Computational Study of Supersonic Turbulent-Separated Flows Using Partially Averaged Navier-Stokes Method, *Acta Astronautica*, 107, 2015, 234–246.
[22] Jung, Y.K., Chang, K., Bae, J.H. Uncertainty Quantification of GEKO Model Coefficients on Compressible Flows, *International Journal of Aerospace Engineering*, 2021, 2021, 1-17.
[23] Herrin, J.L., Dutton, J.C., Supersonic Base Flow Experiments in the Near Wake of a Cylindrical Afterbody, *AIAA Journal*, 32(1), 1994, 77–83.
[24] Reedy, T.M., Elliott, G., Dutton, J.C., Lee, Y., Passive Control of High-Speed Separated Flows Using Splitter Plates, *AIAA Paper 2011-484*, 2011.
[25] Sandberg, R.D., Stability Analysis of Axisymmetric Supersonic Wakes Using Various Basic States, *Journal of Physics: Conference Series 318*, 2011, 032017.
[26] Givoli, D., Non-Reflecting Boundary Conditions, *Journal of Computational Physics*, 94, 1991, 1-29.
[27] Sanderberg, R.D., Fasel, H.F., Numerical Investigation of Transitional Supersonic Axisymmetric Wakes, *Journal of Fluid Mechanics*, 563, 2006, 1-41.
[28] Menter, F.R., Zonal Two-Equation k-w Turbulence Model for Aerodynamic Flow, *AIAA Paper 1993-2906*, 1993.
[29] Lipanov, A.M., Kisarov, Yu.F., Klyuchnikov, I.G., Theoretical Investigation of Parameters for Turbulent Subsonic Flows in Compressible Media: Method and Certain Results, *Doklady Physics*, 44(6), 1999, 380-384.
[30] Karskanov, S.A., Lipanov, A.M., On Critical Reynolds Numbers in Plane Channels with a Sudden Expansion at the Entry, *Computational Mathematics and Mathematical Physics*, 50(7), 2010, 1195-1204.
[31] Jiang, G.S., Shu, C.W., Efficient Implementation of Weighted ENO Schemes, *Journal of Computational Physics*, 126(1), 1996, 202–228.
[32] Shu, C.W., High Order ENO and WENO Schemes for Computational Fluid Dynamics, High-Order Methods for Computational Physics, *Lecture Notes in Computational Science and Engineering*, 9, 1999, 439-582.
[33] Gottlieb, S., Shu, C.W., Total Variation Diminishing Runge-Kutta Schemes, *Mathematics of Computation*, 67, 1998, 73–85.
[34] Lipanov, A.M., Karskanov, S.A., Galactic Structures in a Viscous Gas Flow in a Channel, *Mathematical Models and Computer Simulations*, 11(2), 2019, 168–175.
[35] Pope, S.B., *Turbulent Flows*, Cambridge University Press, 2000.
[36] Menter, F.R., Kuntz, M., Langtry, R., Ten Years of Industrial Experience with the SST Turbulence Model, *in: Turbulence Heat and Mass Transfer 4*, Hanjalic, K., Nagano, Y., Tummers, M.J. (Eds.), Begell House, New York, 2003.
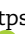
ORCID iD

Sergey A. Karskanov https://orcid.org/0000-0002-1200-8486
Alexander I. Karpov https://orcid.org/0000-0001-8380-1599
Artem A. Shaklein https://orcid.org/0000-0002-3603-4443
Alexey M. Lipanov https://orcid.org/0000-0003-2289-6808
Ivan G. Rusyak https://orcid.org/0000-0001-8584-8884
Stanislav A. Korolev https://orcid.org/0000-0002-8399-1385

Publisher's Note Shahid Chamran University of Ahvaz remains neutral with regard to jurisdictional claims in published maps and institutional affiliations.